ISSN 1063-7834, Physics of the Solid State, 2017, Vol. 59, No. 2, pp. 368–377. © Pleiades Publishing, Ltd., 2017.
Original Russian Text © G.I. Svirskiy, N.N. Sergeeva, S.A. Krasnikov, N.A. Vinogradov, Yu.N. Sergeeva, A.A. Cafolla, A.B. Preobrajenski, A.S. Vinogradov, 2017, published in Fizika Tverdogo Tela, 2017, Vol. 59, No. 2, pp. 357–366.

LOW-DIMENSIONAL SYSTEMS

# Electronic Structure of Nickel Porphyrin NiP: Study by X-Ray Photoelectron and Absorption Spectroscopy

**G. I. Svirskiy[a], N. N. Sergeeva[b], S. A. Krasnikov[a, c], N. A. Vinogradov[a, d], Yu. N. Sergeeva[e], A. A. Cafolla[c], A. B. Preobrajenski[a, d], and A. S. Vinogradov[a, *]**

[a] *Saint Petersburg State University, Universitetskaya nab. 7/9, St. Petersburg, 199034 Russia*
[b] *School of Chemistry, University of Leeds, Leeds, LS2 9JT, UK*
[c] *School of Physical Sciences, Dublin City University, Glasnevin, Dublin 9, Republic of Ireland*
[d] *MAX IV Laboratory, University of Lund, PO Box 118, SE-22100, Lund, Sweden*
[e] *Commissariat à l'Énergie Atomique et aux Énergies Alternatives, Institut Nanosciences et Cryogénie, 17 rue des Martyrs, 38054 Grenoble Cedex 9, France*
** e-mail: asvinograd@gmail.com*

Received June 22, 2016

**Abstract**—Energy distributions and properties of the occupied and empty electronic states for a planar complex of nickel porphyrin NiP are studied by X-ray photoemission and absorption spectroscopy techniques. As a result of the analysis of the experimental spectra of valence photoemission, the nature and energy positions of the highest occupied electronic states were determined: the highest occupied state is formed mostly by atomic states of the porphine ligand; the following two states are associated with 3*d* states of the nickel atom. It was found that the lowest empty state is specific and is described by the σ-type $b_{1g}$ MO formed by empty Ni3$d_{x^2-y^2}$-states and occupied 2*p*-states of lone electron pairs of nitrogen atoms. This specific nature of the lowest empty state is a consequence of the donor–acceptor chemical bond in NiP.

**DOI:** 10.1134/S1063783417020299

## 1. INTRODUCTION

Modern interest in molecular metal–porphyrin (MPs) complexes is caused by their key role in various biochemical processes and the wide use in many technological applications [1]. Porphyrins of transition 3*d* metals (3*d* MPs) are among the most favorable candidates for wide application in molecular electronics [2], nonlinear optics [3], catalysis [4], cancer diagnostics and therapy [5], sensorics [6], and many other directions of modern technologies.

One of the simplest porphyrins of 3*d* metals is nickel (II) porphyrin NiP whose electronic structure, according to optical experiments [7, 8] and quantum chemical calculations [9, 10], is characterized by complete electron shells. Therefore, the total spin of the NiP molecule ground state is zero, which substantially simplifies the analysis and interpretation of spectroscopic data.

It should also be noted that the NiP molecule is a parent of a large family of nickel porphyrin derivatives produced by attaching various functional groups to the NiP periphery. Such a chemical functionalization of the simplest nickel porphyrin significantly extends the spectrum of useful properties of its family. In view of the foregoing, it is clear that comprehensive experimental and theoretical studies of the NiP atomic and electronic structure are very important to understand the properties of this complex and, in essence, represent the necessary first step in the study of electronic properties of nickel porphyrin derivatives and more complex porphyrins of 3*d* metals with partially filled electron shells. A special place in these studies should be given to the experimental study of the total spectrum of occupied and empty NiP electronic states, which controls all physicochemical properties of the compound under study.

So far, the properties of the nickel porphyrin electronic subsystem were mostly experimentally studied using optical absorption spectroscopy methods in UV, visible, and IR regions [11, 12]. However, such experiments do not provide obtaining necessary information about occupied and empty electronic states in nickel porphyrins, since it is indirectly contained in optical spectra in the form of energies and oscillator strengths of observed electronic transitions. The identification of absorption bands in optical spectra of the NiP complex and its derivatives is complicated due to the complex atomic-orbital composition of molecular orbitals (MO) between which electronic transitions occur and is almost impossible without quantum chemical calculations the electronic structure of com-

plexes. Furthermore, transitions of valence electrons with energies of several electronvolts between occupied and empty states arranged only near the Fermi level correspond to optical absorption bands.

On the contrary, X-ray absorption spectra are formed by electronic transitions from inner shells of atoms forming a polyatomic system (a molecule or a complex). As a result, the initial state of the X-ray transition, localized on an individual atom, is described by the atomic orbital (AO) with certain angular symmetry, which significantly simplifies the identification of the final molecular state (MO) and the entire analysis of the fine structure of X-ray absorption spectra. The X-ray absorption spectroscopy method based on the analysis of the near-edge X-ray absorption fine structure (NEXAFS) [13] is among the most informative methods and is currently widely used to study polyatomic systems due to its sensitivity to such details of the local electronic and atomic structure of the system as the ordering, binding energy, atomic-orbital composition, and angular symmetry of the empty electronic states, bond lengths and angles, nearest neighborhood coordination, etc.

In turn, X-ray photoelectron spectroscopy is a modern and widely accepted technique for probing occupied electronic states in polyatomic systems [14]. In studying the spectrum of electronic states and characterizing the chemical bond in the compound, as a rule, inner-shell X-ray photoelectron spectroscopy (XPS) and valence band photoemission (VB-PE) are used.

Several studies are known, in which XPS spectra were measured with low energy resolution and, along with optical absorption spectra, were used to characterize the electronic structure and chemical bonding in nickel porphyrins [15, 16]. Valence photoemission measurements for NiP are absent in the literature. The number of X-ray absorption studies of nickel porphyrins is also small in number; as a rule, they are restricted to an analysis of the narrow initial region of absorption spectra, which reflects the interaction of the nickel atom with pyrrole nitrogen atoms [17–20].

The main objective of this study is to obtain detailed information about the energy distribution, angular symmetry, localization, and atomic-orbital composition of occupied and empty electronic states in the molecular complex of nickel porphyrin NiP by X-ray photoelectron and absorption spectroscopy methods.

## 2. EXPERIMENTAL

All measurements were performed using the equipment of the Russian–German beamline of synchrotron radiation (SR) output and monochromatization of the BESSY II electron storage ring (Berlin, Germany) [21] and the D1011 beamline of SR output and monochromatization of the MAX-II electron storage ring (Lund, Sweden) [22] under close experimental conditions. Nickel porphyrin NiP and free-base (without metal atom) porphine $H_2P$ were synthesized using techniques known from the literature [23]. Samples for measurements represented polycrystalline NiP layers ~30 nm thick, prepared in situ by thermal evaporation of porphyrin powder from a tantalum crucible of a Knudsen cell and deposition on a clean surface of a copper plate. The crucible temperature during deposition was ~600 K. The deposition rate measured by a quartz monitor was ~0.6 nm/min. The porphyrin vapor pressure in the preparation chamber during deposition did not exceed $5 \times 10^{-8}$ mbar. The free porphine $H_2P$ sample was prepared under the same experimental conditions.

X-ray photoelectron spectra for the valence band and core levels (Ni2*p*, N1*s*, and C1*s*) of nickel porphyrin were measured using a Phoibos 150 (Specs GmbH) hemispherical electron analyzer in the mode of recording the normal total photoemission. The total energy resolution (of monochromator and analyzer) for the valence photoemission spectra measured using exciting photons with an energy of 72–170 eV was ~200 meV. The core level spectra were excited by photons with energies of 400, 500, and 940 eV; the total energy resolution was 300, 350, and 700 meV, respectively. NEXAFS spectra of studied porphyrins were obtained by the method of the total electron yield of the external X-ray photoelectric effect in the mode of measurements of the drain current from the sample with varying the energy of photons incident on the sample at an angle of 45°. The monochromator energy resolution in the regions of Ni2$p_{3/2}$ (~850 eV), N1*s* (~400 eV), and C1*s* (~280 eV) absorption edges was 550, 180, and 110 meV, respectively.

All photoemission and absorption spectra were normalized to the incident photon flux monitored by recording the photocurrent from a gold mesh placed at the output of the SR extraction beamline. The photon energy in the range of 70–500 eV was calibrated using Au4$f_{7/2}$, C1*s*, and N1*s* photoelectron (PE) spectra measured with radiation reflected by a diffraction grating in the first and second diffraction orders. The high-energy spectral region was calibrated using the first narrow peak (683.9 eV) in the F1*s* absorption spectrum of solid-phase $K_2TiF_6$ [24]. The PE spectra for the valence band and core levels were approximated using the FitXPS program [25].

All measurements were performed at room temperature and a residual gas pressure in the experimental chamber no more than $2 \times 10^{-10}$ mbar. During measurements, no noticeable effects of charging the samples irradiated with the intense beam of monochromatized SR of the soft X-ray region were observed.

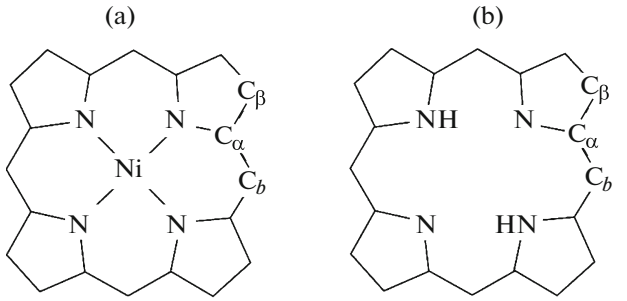


**Fig. 1.** Schematic diagram of (a) nickel porphyrin NiP and (b) free-base porphine $H_2P$ molecules.

## 3. RESULTS AND DISCUSSION

Nickel porphyrin (NiP, $C_{20}H_{12}N_4Ni$) represents a molecular complex consisting of a central complexing nickel atom and a stable ligand representing a porphine macrocycle. The latter is formed by four pyrrole rings $NC_4$ arranged in the same plane and linked by carbon atoms $C_\alpha$ via bridging carbon atoms $C_b$ (Fig. 1) [9]. As a result, the NiP complex is planar and its atomic structure is characterized by $D_{4h}$ point symmetry group. Electronic properties of the nickel porphyrin complex are determined by the electronic structure of the nickel atom and covalent porphine macrocycle, and their chemical interaction. Covalent bonding of the nickel atom with the macrocycle is of donor–acceptor nature and is implemented by displacing the lone 2*p* electron pair of the nitrogen atom of each pyrrole group to the empty 3*d* orbital of the nickel atom [15]. As a result, four $sp^2d$-hybridized σ-bonds are formed, which provide square coordination of the nitrogen atoms around the nickel atom.

The electronic spectrum of the polyatomic system (molecule, complex) can be described using the spectral distribution of bonding and antibonding one-electron MOs of this system, which, as a rule, characterize occupied and empty electronic states of the polyatomic system, respectively. In the case of a planar molecule, these MOs are differently oriented with respect to the molecular plane: σ-type MOs are arranged in the molecule plane, and π-type MOs are perpendicular to it [26]. As a rule, π-bonding is weaker in comparison with σ-bonding, which leads to lower bond energies for bonding and antibonding π-type MOs.

In the condensed state, NiP represents a molecular crystal in which intermolecular cohesion is characterized by the weak Van der Waals interaction [27]. As a result, the electronic structure of the nickel porphyrin crystal is controlled to a large extent by the electronic electrical of an individual molecule. Thus, the valence band and conduction band of the NiP crystal can be described in sufficient detail by separate narrow subbands originating from one-electron MOs, describing occupied and empty electronic states of one NiP molecule.

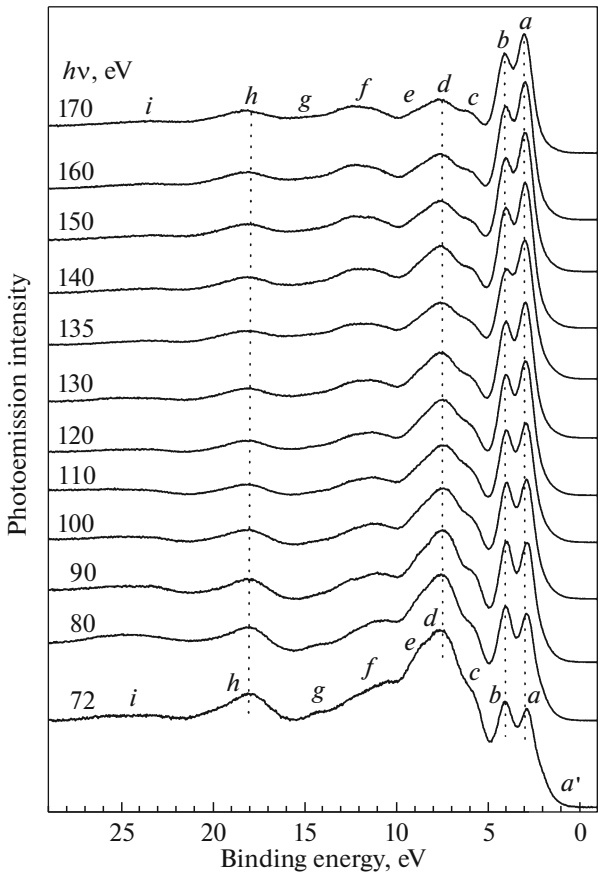


**Fig. 2.** Valence-band photoemission spectra of nickel porphyrin NiP, measured at various energies of exciting photons in the range from 72 to 170 eV.

We begin the discussion of the obtained experimental results with the consideration of valence photoemission spectra of nickel porphyrin, measured at various energies *hν* of exciting photons in the range from 72 to 170 eV (Fig. 2). The photoemission spectra normalized to the incident radiation intensity are presented on the scale of valence electron binding energies relative to the Fermi level. The intensity of the photoelectron signal in the region of negative binding energies are almost zero for each spectrum.

All spectra contain two narrow lines *a* and *b* near the Fermi level with bond energies of 2.9 and 4.1 eV, respectively, and wider PE bands *c*–*i* at higher energies. Furthermore, the spectra measured at exciting photon energies *hν* = 72–110 eV contain a noticeable shoulder *a*' of line *a*, which is less distinct in other spectra. It should be noted that all PE bands retain their energy positions with varying exciting photon energies, hence, they are caused by photoionization of the upper occupied electronic states which can be

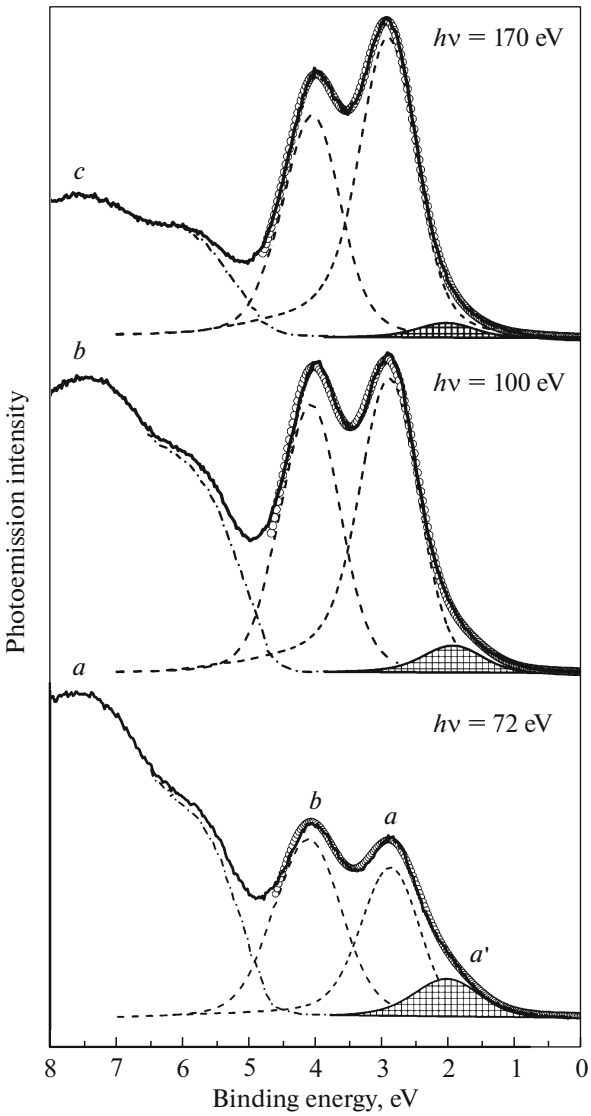


**Fig. 3.** Approximation of the valence-band photoemission spectra of nickel porphyrin in the binding energy range of 0–8 eV using lines *a*', *a*, and *b* for the spectra measured at photon energies of (*a*) 72, (*b*) 100, and (*c*) 170 eV. The experimental curve is shown by a continuous solid curve. Lines *a* and *b* in the expansion are dashed, the line *a*' profile is shaded. The dash-dotted curve shows the contribution of nearby photoelectron bands *c* and *d* to the analyzed spectral region. The final approximation result is shown by open circles.

described by occupied one-electron MOs of the complex under study.

Comparing the valence photoemission spectra of nickel porphyrin, we note that the intensity of *c*–*i* bands monotonically decreases several times with increasing exciting photon energy $h\nu$, approximately retaining their relative values in the spectra. At the same time, a significant increase in the relative intensities of lines *a* and *b* is observed in the considered spectra: they increase approximately by a factor of 4 with respect to band *d* (with background) as the exciting photon energy increases from 72 to 170 eV. Furthermore, line *a* gradually becomes more intense than line *b*.

The isolated character of bands *a* and *b* allows approximation of the valence PE spectra near the Fermi level ($E_{bind}$ = 0–8 eV) using three lines *a*', *a*, and *b*; the results of this approximation for three spectra measured with exciting photon energies of 72, 100, and 170 eV are shown in Fig. 3. It is easily seen that the relative intensity of line *a*' at the binding energy of 2.0 eV in comparison with line *a* monotonically decreases from 0.26 to 0.05 as the photon energy increases from 72 to 170 eV (the results of approximation for other valence photoemission spectra, not shown in the figure, are consistent with this statement). Along with this, the ratio of the intensities of peaks *b* and *a* changes in favor of the latter. Thus, line *a*' behaves with increasing energy $h\nu$ similarly to bands *c*–*i*. This observation unambiguously indicates the close atomic-orbital composition of occupied MOs responsible for bands *c*–*i* and *a*' and points to significant differences between these orbitals and MOs characterizing occupied electronic states *a* and *b*.

Indeed, variations of the spectral profile of valence photoemission, observed with increasing $h\nu$ reflect spectral variations in the photoionization cross section of upper occupied MOs of the NiP complex. These photoionization cross sections are determined, in turn, by the corresponding cross sections for valence electron shells of atoms composing the molecular complex, i.e., partial N3*d* N2*p*, and C2*p* photoionization cross sections. To estimate the changes in these values, we turn to photoionization cross sections calculated for various atomic electron shells in the photon energy range $h\nu$ from 0 to 1500 eV [28]. We find that the photoionization cross sections for N2*p* and C2*p* shells at $h\nu \sim 70$ eV are about 1.3 and 0.5 Mb, respectively, whereas the cross section for the Ni3*d* shell is ~8.5 Mb. As the photon energy increases to 170 eV, all compared cross sections monotonically decrease to 0.1 Mb (N2*p*), 0.04 Mb (C2*p*), and 3 Mb (Ni3*d*). In other words, as the photon energy increases from 72 to 170 eV, the photoionization cross sections of N2*p* and C2*p* electron shells decrease by a factor of ~13, and the cross section of the nickel atom decreases only by a factor of 3, i.e., more than four times slower than 2*p* photoionization cross sections of nitrogen and carbon atoms.

These differences in the decrease rate of the calculated photoionization cross sections of valence electron shells of the nickel atom, on the one hand, and carbon and nitrogen atoms, on the other hand, correlate with changes in the relative intensities of lines *a* and *b* in comparison with bands *a*' and *c*–*i* in experimental spectra as the exciting photon energy increases from 72 to 170 eV. This fact allows the assumption that PE lines *a* and *b* are related to nickel porphyrin MOs

formed mostly by 3*d* orbitals of the nickel atom, and bands *a*' and *c*–*i* reflect MOs of the porphine macrocycle in which the contributions of valence orbitals of carbon and nitrogen atoms dominate. We note that the observed smaller energy width of lines *a* and *b* in comparison with bands *c*–*i* is in agreement with the above considerations about the relation of these PE lines with occupied 3*d* states of the nickel atom. Indeed, 3*d*-electrons are highly localized within the nickel atom as a result of electron shell collapse [29]; as a result, their states cannot differ significantly (disperse) in energy. We also note that high-energy PE bands *h* and *i* with binding energies of 18 and 24.5 eV are most likely related to MOs formed mostly by C2*s* and N2*s* AOs whose calculated binding energies in free atoms are 17.5 and 23.1 eV, respectively [28].

The free nickel atom with $[Ar]3d^8 4s^2$ electronic configuration in the NiP complex appears as a divalent atom Ni(II) which, within the formal valence concepts has $[Ar]3d^8$ electronic configuration of the $Ni^{2+}$ ion. In the field of the square NiP complex ($D_{4h}$ symmetry group), fivefold degenerate 3*d* states of the nickel ion are split (in increasing energy order) into one doubly degenerate $e_g(3d_{xz,\ yz})$ state and three nondegenerate $a_{1g}(3d_{z^2})$, $b_{2g}(3d_{xy})$, and $b_{1g}(3d_{x^2-y^2})$ states [30]. In this case, three lower 3*d*-states are occupied by electrons ($e_g^4$, $a_{1g}^2$, and $b_{2g}^2$), and the energetically highest state $b_{1g}$ remains empty. Atomic 3*d*-orbitals of nickel describing these states are involved, in addition to 2*p*-orbitals of nitrogen atoms of the porphine ligand, in the formation of σ- and π-type MOs ($a_{1g}$, $b_{1g}$ and $b_{2g}$, $e_g$, respectively) which characterize chemical bonding between the nickel atom and ligand in the complex.

Taking into account the assumption about the relation between PE lines *a* and *b* with occupied MOs having large contributions of Ni3*d* states, it is reasonable to consider three occupied MOs $e_g$, $a_{1g}$, and $b_{2g}$ to be responsible for these lines in the valence photoemission spectrum. The intensities of lines *a* and *b* are not significantly different from each other, hence, these lines are related to MOs having close contributions of Ni3*d* states. Therefore, we can suggest that line *a* is characterized by two nondegenerate states $a_{1g}$ and $b_{2g}$ having close binding energies, and line *b* is characterized by one doubly degenerate state $e_g$.

Let us compare the conclusions about the nature of upper occupied MOs in nickel porphyrin with the results of calculations performed for this complex within the density functional theory (DFT) [9]. First of all, we note that the energy sequences of occupied MOs with dominant Ni3*d* contributions in DFT calculations ($b_{2g}$, $e_g$, and $a_{1g}$) and the crystal field theory ($e_g$, $a_{1g}$, and $b_{2g}$) are not identical. This indicates the important role of the chemical bonding effects and electron charge transfer processes between the nickel atom and porphine ligand in the formation of the spectrum of occupied electronic states in NiP.

According to the calculations, the upper occupied MOs in NiP are the highest occupied MO (HOMO) $a_{1u}$ and the following HOMO-1 $a_{2u}$ that have binding energies identical within 0.01 eV. These MOs are localized on pyrrole rings of the porphine ligand and are characterized by dominant contributions of 2*p* AOs of pyrrole carbon atoms ($C_\alpha$ and $C_\beta$) for HOMO and 2*p*-AOs of the nitrogen atom and bridging carbon atom $C_b$ for HOMO-1. It is clear that these MOs correspond to PE band *a*' in the experimental spectrum (Fig. 3).

Then, at higher binding energies, two neighboring MOs of $a_{1g}$ and $e_g$ symmetry are found according to the calculation, which have dominant contributions of $Ni3d_{z^2}$ and $Ni3d_{xz,\ yz}$ orbitals. Taking into account the smallness of the energy distance $\Delta E$ between these MOs (0.01 eV), it is reasonable to consider that they are responsible for line *a* in the valence photoemission spectrum. Two more MOs of $b_{2g}$ and $e_g$ symmetry with Ni3*d* contributions almost identical in energy ($\Delta E$ = 0.01 eV) are even deeper. The first $b_{2g}$ MO is essentially a pure $3d_{xy}$ nickel atom orbital, whereas the second contains contributions of $Ni3d_{xz,\ yz}$, N2*p*, and $C_\beta 2p$ orbitals in close fractions. This allows the conclusion that line *b* is mostly characterized by the MO of $b_{2g}$ symmetry. We note that lines *a* and *b* within this calculation are related to other components of 3*d* AOs of the nickel atom, rather than it was assumed based on an analysis of experimental valence photoemission spectra.

In addition to the aforementioned MOs, the cited calculation indicates the existence of four more states in the nickel porphyrin valence spectrum, which are described by MOs of $b_{2u}$, $a_{2u}$, $e_u$, and $b_{2g}$ symmetry and are localized on the porphine macrocycle. The first two MOs are energetically arranged between the orbitals responsible for photoelectron lines *a* and *b*, and the second two MOs have binding energies slightly higher than state *b*.

The results of the comparison of the calculated data with the experimental spectrum of NiP valence photoemission, unfortunately, make it possible to consider only their qualitative agreement: the highest occupied state is localized on the porphine macrocycle; below, the states with Ni3*d* contributions are located, and then the porphine ligand states follow again. The quantitatively compared data are not quite consistent. Indeed, the experimental spectrum of NiP valence states (bands *a*'–*g*, Fig. 2) has an energy width of ~12 eV, whereas the width of the theoretical spectrum is only 4.3 eV. For compared spectra, this is also accompanied by differences in the sequence order of MOs localized on the nickel atom and porphine macrocycle and in their relative energy positions. For example, the energy distance between lines *a*' and *a* and in the experimental spectrum is 0.9 eV, while the distance between corresponding MOs in the calcula-

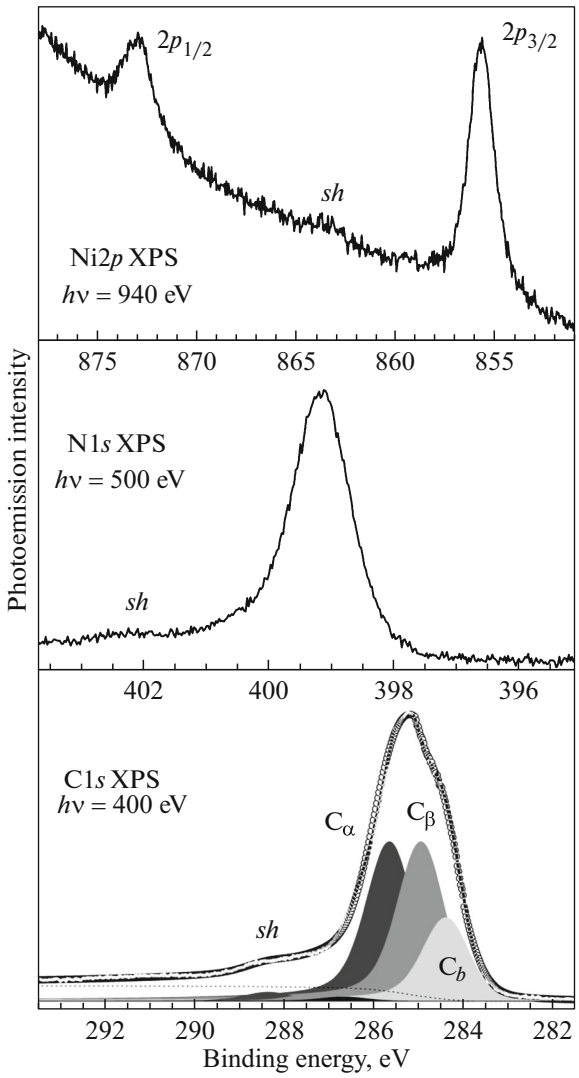


**Fig. 4.** Ni2*p*, N1*s*, and C1*s* photoelectron spectra of nickel porphyrin NiP. The approximation for the C1*s* spectrum: the experimental curve is solid, contours of photoelectron lines corresponding to carbon atoms in different chemical states ($C_b$, $C_\alpha$, $C_\beta$) are painted, the dashed curve is the background, and the final spectrum is shown by open circles.

tion is only 0.3 eV. MOs of the porphine ligand are arranged between MOs with Ni3*d* contributions in the calculation, which seems improbable according to the shape of lines *a* and *b*.

At the same time, it should be noted that the theoretical energy splitting between two MOs $\{a_{1g} + e_g$ and $b_{2g}\}$ with Ni3*d* contributions is ~1.3 eV, which is in good agreement with the experimental energy distance of 1.2 eV between lines *a* and *b*.

Finally, let us compare the relative intensities of experimental lines *a* and *b* with their ratio expected from calculations. According to the latter, the intensity of line *a* is controlled by Ni3*d* contributions to MOs of $a_{1g}$ and $e_g$ symmetry (0.97 and 0.71, respectively), and line *b* is controlled by the corresponding contribution to the $b_{2g}$ MO (0.93). Taking into account these values and double degeneracy of MOs of $e_g$ symmetry, the ratio of 2.57 : 1 is expected from the calculation for the intensities of lines *a* and *b*. Comparing this ratio with the values obtained from experimental spectra, i.e., 0.84 : 1 ($h\nu = 72$ eV), 1.08 : 1 ($h\nu = 100$ eV), and 1.33 : 1 ($h\nu = 170$ eV), we come to the conclusion about poor agreement between the experiment and cited calculation.

Completing the comparative analysis of the experimental data and the DFT calculation [9] for upper occupied electronic states in NiP, we note that different sequences of upper occupied MOs are presented in the calculations [9, 31] performed by the same group. This disagreement is explained by differences in the chosen approximation for the exchange potential. The ambiguity of the results of DFT calculations for nickel porphyrin is also indicated by the data of [10] in which the calculated sequence of upper occupied MOs differs from the MO sequence in the aforementioned studies.

Let us now take a brief look at X-ray photoelectron spectra (XPS) of core Ni2*p*, N1*s*, and C1*s* electrons (Fig. 4), which contain information about the chemical state of atoms in NiP and are necessary for energy alignment of the absorption spectra of various atoms on a unified energy scale. The measured XPS spectra are shown on the scale of binding energies measured relative to the Fermi level. The Ni2*p* spectrum consists of two spin-doublet components, i.e., $Ni2p_{1/2}$ and $Ni2p_{3/2}$ at binding energies of 873.0 and 855.7 eV, respectively. These values are significantly higher than binding energies of $2p_{1/2}$ and $2p_{3/2}$ electrons with respect to the Fermi level in metal nickel (870.0 and 852.7 eV) [32], which indicates the significant transfer of the electron density from the nickel atom to the porphine ligand in NiP. The $Ni2p_{3/2}$ spectrum at the binding energy of 863.5 eV contains the distinct high-energy satellite *sh* indicating the appreciable role of multielectron (shake-off) effects during photoionization of the $2p_{3/2}$ electron shell of the nickel atom [33]. The photoelectron N1*s* spectrum is also characterized by the simple-shaped single line at the binding energy of 399.15 eV, which indicates the identical chemical state of all nitrogen atoms in the complex. The weak high-energy satellite *sh* at the energy of 402.3 eV reflects the existence of shake-off processes during photoionization of the N1*s* shell [34].

In contrast to the spectra of nickel and nitrogen, the C1*s* spectrum has a more complex asymmetric profile that can be approximated by three components $C_\alpha$, $C_\beta$, and $C_b$ which correspond to three types of carbon atoms presenting in NiP in different chemical states (Fig. 1). The relative intensities of these components reflect the number of various carbon atoms in the complex $C_\alpha : C_\beta : C_b = 2 : 2 : 1$, and their energies,

285.65 eV ($C_\alpha$), 284.95 eV ($C_\beta$), and 284.38 eV ($C_b$), reflect the chemical (charge) state of these carbon atoms in nickel porphyrin. Noticeable differences of the energies of C1*s* electrons characterize the values and directions of the electron transfer between carbon atoms, caused by the presence of the more electronegative nitrogen heteroatom in the pyrrole ring.

To obtain information about empty electronic states in NiP and their properties, we consider the near-edge fine structure of the X-ray absorption spectra (NEXAFS) of the complex in the region of Ni2*p*, N1*s*, and C1*s* ionization thresholds (Fig. 5). The designations of the absorption bands in the spectra are given in view of the results of their subsequent identification. The measured 2*p* absorption spectrum of the nickel atom consists of $2p_{3/2}$ and $2p_{1/2}$ components caused by spin–orbit splitting of the initial Ni2*p* state (17.3 eV [32]). The fine structure of these spectra is formed mostly by dipole-allowed transitions of $2p_{3/2}$ and $2p_{1/2}$ electrons to empty MOs with involvement of 3*d* states of the nickel atom, since allowed transitions of 2*p*-electrons to 4*s* states is less intense than transitions to 3*d* states by a factor of ~20 [35]. In what follows, we restrict the consideration to only the low-energy $2p_{3/2}$ component having a more distinct and intense structure. In the $2p_{1/2}$ spectrum, the structure is resolved much lower, since the initial Ni$2p_{1/2}$ level in comparison with the Ni$2p_{3/2}$ level has a substantially larger intrinsic width due to the existence of the additional Auger-$2p_{1/2}2p_{3/2}3d$ decay process for the Ni$2p_{1/2}$ vacancy [36].

For C1*s* and N1*s* absorption spectra of NiP and $H_2P$, the presence of two regions with different absorption structures is characteristic, i.e., the low-energy region with narrow lines and the high-energy region with broad absorption bands. Lines *B*–*C* in N1*s* spectra (*B*–$B_2$ in C1*s* spectra) of NiP and $H_2P$ differ appreciably in shapes and energy positions, whereas high-energy absorption bands *D*–*F* in nitrogen spectra and *C*–*F* in carbon spectra are almost identical in shapes and energy positions in the compared spectra.

It is conventional to describe the near-edge fine structure of X-ray absorption spectra using multiple (resonant) scattering of photoelectrons ejected from atoms due to X-ray photon absorption on nearest neighbor atoms [13, 24]. At certain photoelectron energies, a quasi-molecule formed by neighborhood atoms can temporarily trap a photoelectron, resulting in the formation of metastable states (shape resonances) for it. These resonances, depending on their lifetime, are observed in the spectra as narrow lines or broad absorption bands. Resonance localization in the quasi-molecule field allows us to consider them as a result of dipole-allowed transitions of core electrons to empty electronic states of this polyatomic system, which are described by its unoccupied MOs.

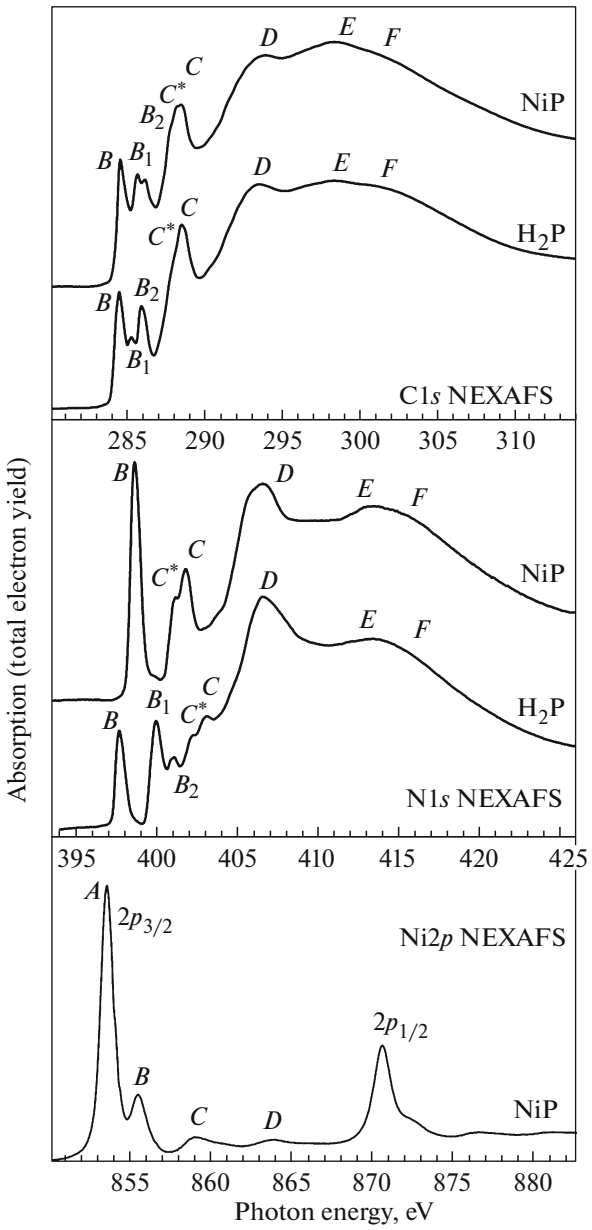


**Fig. 5.** Ni$2p_{3/2}$, N1*s*, and C1*s* absorption spectra of nickel porphyrin NiP. For comparison, N1*s* and C1*s* absorption spectra of free-base porphine $H_2P$ are shown.

Within this approach to the description of NEXAFS spectra, it is reasonable to assert that the differences in the low-energy region of NEXAFS spectra of NiP and $H_2P$ reflect differences in their local electronic structure, which are caused by changes in central atoms of the complex and the nature of their chemical bonding with neighboring nitrogen atoms of the porphine ligand in NiP in comparison with $H_2P$. In turn, the high-energy absorption bands in the spectra of both complexes are related to the fine structure formation processes within the rigid porphine ligand which changes slightly during the transition from NiP

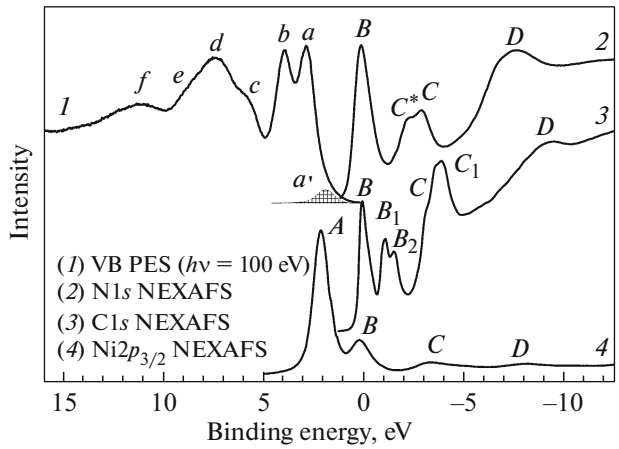


**Fig. 6.** Valence-band photoemission spectrum VB PES ($h\nu = 100$ eV) and Ni2$p_{3/2}$, N1$s$, and C1$s$ absorption spectra of nickel porphyrin NiP, aligned in energy on a common scale of binding energies reletive to the Fermi level.

to $H_2P$. It is clear from the above comparison that information about features of the local electronic structure of the complex, caused by chemical bonding of the nickel atom with the porphine ligand, is contained mostly in the low-energy region of absorption spectra.

Let us consider the informative region of the NiP absorption spectra within the quasi-molecular approach, assuming that the local electronic structure of the complex is essentially determined by the polyatomic group (quasi-molecule) $NiN_4(C_\alpha)_8$ that forms the central complexing nickel atom with nitrogen and carbon atoms of the first and second coordination spheres of its neighborhood (Fig. 1). This quasi-molecule, as the nickel porphyrin molecule as a whole, is characterized by $D_{4h}$ point symmetry group. In this approach, the fine structure of the compared absorption spectra of the polyatomic system under study can be considered uniformly as a result of dipole-allowed transitions of core electrons to the common system of unoccupied electronic states of the complex, which can be approximated by empty quasi-molecule MOs [24].

In Fig. 6, the low-energy region of NiP absorption spectra is shown together with the valence-band photoemission spectrum ($h\nu = 100$ eV) on the common scale of the binding energy determined relative to the Fermi level. The absorption spectra are aligned in energy on this scale, using the binding energies for Ni2$p_{3/2}$, N1$s$, and $C_\alpha$1$s$ electrons considered above, i.e., 855.7, 399.15, and 285.65 eV, respectively. We note that the binding energy of $C_\alpha$ atoms directly interacting with nitrogen atoms in the complex and incorporated in the used quasi-molecule was taken in the case of the carbon spectrum. The consideration of the fine structure of the absorption spectra aligned in energy on a common energy scale within the quasi-molecular approach implies the identity of the energy positions of absorption lines and bands related to transitions to the same MOs in the compared spectra.

From the energetically aligned NiP spectra, we note first of all that the absorption resonance $A$ corresponding to the lowest empty state of the complex is observed only in the Ni2$p_{3/2}$ absorption spectrum. This immediately suggests that this state is characterized by the lowest unoccupied MO (LUMO) of $b_{1g}$ symmetry with the contribution of $3d_{x^2-y^2}$ states of the nickel atom, which remain unoccupied for the divalent Ni(II) atom in the molecular field of the square ($D_{4h}$) complex. According to the calculations [9, 10], the LUMO in NiP is a weakly antibonding σ-type $b_{1g}$ MO in which, along with Ni$3d_{x^2-y^2}$ AO, 2$p$ states of nitrogen atoms make an appreciable contribution. However, no trace of any structure similar to the $A$ band in the Ni2$p_{3/2}$ spectrum is in the N1$s$ absorption spectrum. In [20], to explain this observation, it was assumed that the actual contribution of N2$p$ states to the LUMO is significantly smaller than the calculated value (~0.33) [10, 31]. At the same time, it should be noted that the energy position of the $A$ peak falls exactly on the band $a'$ in the valence photoemission spectrum, which reflects the upper occupied state of the complex, related to the porphine ligand. Previously, it was attributed to the HOMO and HOMO-1 of $a_{1u}$ and $a_{2u}$ symmetry, almost identical in energy. At first sight, such a correlation of the absorption peak $A$ and photoemission band $a'$ seems improbable.

However, the donor–acceptor mechanism of the formation of the chemical σ-bond in NiP implies the involvement of four nitrogen atoms in bonding by their lone 2$p$ electron pairs. Each pair is displaced to the region of the empty Ni$3d_{x^2-y^2}$ state and forms a two-electron covalent bond between nickel and nitrogen atoms, which differs drastically from the ordinary two-center covalent bond [11]. According to the DFT calculation [9], the HOMO-1 of $a_{2u}$ symmetry has a significant contribution of N2$p$ states that most likely does represent the lone electron pair of the nitrogen atom. Since the photoemission band $a'$ is related to the HOMO-1, its energy correlation with resonance $A$ in the Ni2$p_{3/2}$ absorption spectrum becomes clear. Therefore, it is reasonable to assert that the absence of an analogue of band $A$ in the nitrogen spectrum is caused by the specific composition of the LUMO in whose formation unoccupied Ni3$d$ states are involved along with occupied 2$p$ states of lone electron pairs of nitrogen atoms. In this case, the transitions of N1$s$ electrons in the LUMO are simply impossible, since N2$p$ states in it are occupied.

The next absorption resonance $B$ is clearly observed in all compared NiP absorption spectra, and its energy positions in various spectra are identical within the experimental accuracy (~0.1 eV). From this

it clearly follows that the next LUMO + 1 empty state responsible for the resonance *B* is a molecular state (MO) with contributions of Ni3*d*, N2*p*, and $C_\alpha 2p$ states. The hybridized nature of the LUMO + 1 is confirmed by the calculation [9] according to which this empty state is attributed to π-type $e_g$ MO with a small contribution of Ni3$d_{xz,\ yz}$π states and significant contributions of 2*p*π states of porphine ligand atoms. The calculated characteristics of the second empty state in NiP are in qualitative agreement with experimental results.

Indeed, peaks *B* in the nitrogen (2) and carbon (3) spectra in their shape correspond to the transitions of 1*s* electrons to empty π states of the molecular complex, and their high intensities in comparison with the nickel spectrum reflect the fact, that N2*p* and C2*p* contributions to the LUMO + 1 are several times larger than the contribution of Ni3*d* states [9].

As noted above, 3*d* electrons are highly localized in the intra-atomic region of the nickel atom due to collapse of their electronic shell, which is reflected in the small width of photoelectron lines *a* and *b* in the valence photoemission spectrum of NiP (Fig. 2). At the same time, the significant intensity of band *B* in the nickel absorption spectrum suggests that partial delocalization of 3*d* electrons takes place in this complex. In [19, 20], similar delocalization in nickel porphyrins and phthalocyanine was related to strong π-bonding between nickel and ligand atoms. This bonding is realized due to covalent Ni3$d_{xz,\ yz}$–N,C2*p* mixing and is accompanied by charge transfer of the Ni3*d* electron density to ligand atoms (the back-donation effect [26]). The existence of π-bonding between nickel and ligand atoms in nickel porphine is confirmed by all DFT calculations; however, the calculated transfer of the Ni3*d* electron density (contribution to the LUMO + 1) is small (~0.03) [9] and does not allow us to explain the significant intensity of band *B* in the Ni2$p_{3/2}$ spectrum, which is about one quarter of the intensity of the main transition (resonance *A*) to the LUMO of $b_{1g}$ symmetry with the contribution of Ni3*d* states, equal to 0.59. Then, the calculation is not consistent with the experiment when comparing the energy distance between LUMO and LUMO + 1, $\Delta E(b_{1g}–e_g)$ which is 0.35 eV in the calculation [9] and 2.1 eV in the experiment.

The peaks $B_1$ and $B_2$ are observed only in the C1*s* absorption spectrum of NiP, which points to their relation to empty MOs of the porphine ligand. The energy distance between them of 0.47 eV is identical to the distance of 0.55 eV between $C_\beta$1*s* and $C_b$1*s* levels in nickel porphyrin within the experimental accuracy (~0.1 eV). This allows the assumption that the resonances $B_1$ and $B_2$ in the carbon absorption spectrum reflect the transitions between 1*s* electrons of $C_\beta$ and $C_b$ carbon atoms not directly bound with nickel and nitrogen atoms into the same empty state of the porphine ligand. It is quite possible that this state corresponds to the calculated LUMO + 2 of $b_{1u}$ symmetry, which is mostly localized on $C_\beta$ and $C_b$ carbon atoms and has no contributions of nickel and nitrogen atoms.

Then, in principle, analogues to low-intensity bands *C* and *D* in the Ni2$p_{3/2}$ spectrum in 1*s* nitrogen and carbon spectra can be indicated; however, identification of these bands is complicated at this stage, and it only can be assumed that they are related to the transitions of core electrons to antibonding MOs having contributions of Ni4*s*,4*p* and N,C2*p* states.

## 4. CONCLUSIONS

The energy distributions and properties of occupied and empty electronic states for the planar complex of nickel porphyrin NiP were studied by X-ray photoemission and absorption spectroscopy.

Regularities in the behavior of the valence-band photoemission spectrum with increasing the energy of exciting photons from 72 to 170 eV were analyzed based on the theoretical dependences of the spectral behavior of partial Ni3*d*, N2*p*, and C2*p* photoionization cross sections. As a result, it was found that the highest occupied state of the nickel porphyrin complex with a binding energy of 2.0 eV is characterized by the MO composed of atomic states of the porphine ligand. Slightly deeper, at energies 2.9 and 4.1 eV, occupied MOs of the complex are located, which are formed mostly from Ni3*d* states. In the binding energy range from 5 to 15 eV, occupied MOs of the porphine ligand are located.

Photoelectron Ni2$p_{3/2}$ and N1*s* spectra are characterized by simple-shaped single lines, whereas the C1*s* spectrum has a more complex asymmetric profile. It can be approximated by three components $C_\alpha$, $C_\beta$, and $C_b$ that correspond to three types of carbon atoms in NiP in different chemical states.

A comparative analysis of C1*s* and N1*s* absorption spectra of NiP with spectra of free porphine $H_2P$ showed that the substitution of hydrogen atoms with nickel atoms has no significant effect on the porphine ligand, but affects the chemical state of nitrogen and carbon $C_\alpha$ atoms, which leads to changes in the initial region of the fine structure of N1*s* and C1*s* spectra.

The fine structure of the NiP absorption spectra and the valence-band photoemission spectrum were considered within the quasi-molecular approach on a unified binding energy scale (relative to the Fermi level). As a result, it was found that the lowest unoccupied state LUMO is specific and is described by a σ-type MO formed by empty Ni3$d_{x^2-y^2}$ states and occupied 2*p* states of lone electron pairs of nitrogen atoms. In this case, transitions of Nl*s* electrons to the LUMO are impossible, since N2*p* states in it are occupied. This specific nature of the LUMO is a consequence of the donor–acceptor chemical bond in NiP.

The next unoccupied state LUMO + 1 is attributed to π-type $e_g$-MO with a small contribution of Ni3$d_{xz, yz}$ π states and significant contributions of 2$p$π states of porphine ligand atoms. This π-bonding is realized due to covalent Ni3$d_{xz, yz}$–N, C2$p$ mixing and is accompanied by charge transfer of the Ni3$d$ electron density to ligand atoms (the back-donation effect).

As a result of the direct comparison, it was found that the experimental valence-band photoemission and absorption spectra are consistent with the results of DFT calculations only qualitatively.

## ACKNOWLEDGMENTS

The authors are grateful to M.M. Brzhezinskaya (BESSY) for assistance in measurements.

This study is performed in part within the bilateral program of the Russian-German Laboratory at BESSY and was supported by the Russian Foundation for Basic Research (project no. 15-02-06369).

## REFERENCES

1. *The Porphyrin Handbook*, Ed. by K. M. Kadish, K. M Smith, and R. Guilard (Academic, San Diego, California, United States, 2000), Vols. 1–10.
2. H. L. Anderson, Chem. Commun. (Cambridge), No. 12, 2323 (1999).
3. O. Senge, M. Fazekas, E. G. A. Notaras, W. J. Blau, M. Zawadzka, O. B. Locos, and E. M. Ni Mhuiercheartaigh, Adv. Mater. (Weinheim) **19**, 2737 (2007).
4. P. Bhyrappa, J. K. Young, J. S. Moore, and K. S. Suslick, J. Am. Chem. Soc. **118**, 5708 (1996).
5. Manivannan Ethirajan, Yihui Chen, Penny Joshi, and Ravindra K. Pandey, Chem. Soc. Rev. **40**, 340 (2011).
6. D. Filippini, A. Alimelli, C. Di Natale, R. Paolesse, A. D'Amico, and I. Lundström, Angew. Chem., Int. Ed. **45**, 3800 (2006).
7. M. Gouterman, J. Mol. Spectrosc. **6**, 138 (1961).
8. A. Antipas and M. Gouterman, J. Am. Chem. Soc. **105**, 4869 (1983).
9. A. Rosa, G. Ricciardi, E. J. Baerends, and S. J. A. van Gisbergen, J. Phys. Chem. A **105**, 3311 (2001).
10. M. S. Liao and S. Scheiner, Chem. Phys. **117**, 205 (2002).
11. J. S. Evans and R. L. Musselman, Inorg. Chem. **43**, 5613 (2004).
12. D. Kim, C. Kirmaier, and D. Holten, Chem. Phys. **75**, 305 (1983).
13. J. Stöhr, *NEXAFS Spectroscopy* (Springer Verlag, Berlin, 1992).
14. S. Hüfner, *Photoelectron Spectroscopy: Principles and Applications*, 2nd ed. (Springer-Verlag, Berlin, 1995).
15. C. Berrios, G. I. Cárdenas-Jirón, J. F. Marco, C.Gutiérrez, and M. S. Ureta-Zañartu, J. Phys. Chem. A **111**, 2706 (2007).
16. C. Berrios, J. F. Marco, C. C. Gutiérrez, and M. S. Ureta-Zañartu, J. Phys. Chem. B **112**, 12644 (2008).
17. K. M. Barkigia, M. W. Renner, L. R. Furenlid, C. J. Medforth, K. M. Smith, and J. Fajer, J. Am. Chem. Soc. **115**, 3627 (1993).
18. L. Campbell, S. Tanaka, and S. Mukamel, Chem. Phys. **299**, 225 (2004).
19. S. A. Krasnikov, A. B. Preobrajenski, N. N. Sergeeva, M. M. Brzhezinskaya, M. A. Nesterov, A. A. Cafolla, M. O. Senge, and A. S. Vinogradov, Chem. Phys. **332**, 318 (2007).
20. S. A. Krasnikov, N. N. Sergeeva, M. M. Brzhezinskaya, A. B. Preobrajenski, Y. N. Sergeeva, N. A. Vinogradov, A. A. Cafolla, M. O. Senge, and A. S. Vinogradov, J. Phys.: Condens. Matter **20**, 235207 (2008).
21. S. I. Fedoseenko, I. E. Iossifov, S. A. Gorovikov, J.-S. Schmid, R. Follath, S. L. Molodtsov, V. K. Adamchuk, and G. Kaindl, Nucl. Instrum. Methods Phys. Res., Sect. A **470**, 84 (2001).
22. R. Nyholm, S. Svensson, J. Nordgren, and A. Flodström, Nucl. Instrum. Methods Phys. Res., Sect. A **246**, 267 (1986).
23. E. Unger, U. Bobinger, W. Dreybrodt, and R. Schweitzer-Stenner, J. Phys. Chem. **97**, 9956 (1993).
24. A. S. Vinogradov, S. I. Fedoseenko, S. A. Krasnikov, A. B. Preobrajenski, V. N. Sivkov, D. V. Vyalikh, S. L. Molodtsov, V. K. Adamchuk, C. Laubschat, and G. Kaindl, Phys. Rev. B: Condens. Matter **71**, 045127 (2005).
25. D. L. Adams, *FitXPS: A Fitting Program for Core Level Spectra (Version 2.12)*. http://ww2.sljus.lu.se/download.html.
26. F. Cotton and G. Wilkinson, *Basic Inorganic Chemistry* (Wiley, New York, 1976; Mir, Moscow, 1979).
27. S. R. Forrest, Chem. Rev. **97**, 1793 (1997).
28. J. J. Yeh and I. Lindau, At. Data Nucl. Data Tables **32**, 1 (1985).
29. R. I. Karaziya, Sov. Phys.—Usp. **24** (9), 775 (1981).
30. I. B. Bersuker, *Electronic Structure and Properties of Transition Metal Compounds: Introduction to the Theory*, 3rd ed. (Khimiya, Leningrad, 1986; Wiley New York, 1996).
31. A. Rosa, G. Ricciardi, E. J. Baerends, M. Zimin, M. A. J. Rodgers, S. Matsumoto, and N. Ono, Inorg. Chem. **44**, 6609 (2005).
32. J. C. Fuggle and N. Mårtensson, J. Electron Spectrosc. Relat. Phenom. **21**, 275 (1980).
33. M. C. Biesinger, B. P. Payne, A. P. Grosvenor, L. W. M. Lau, A. R. Gerson, and R. St. C. Smart, Appl. Surf. Sci. **257**, 2717 (2011).
34. M. P. Keane, A. Naves de Brito, N. Correia, and S. Svensson, Chem. Phys. **155**, 379 (1991).
35. H. Ebert, J. Stöhr, S. S. P. Parkin, M. Samant, and A. Nilsson, Phys. Rev. B: Condens. Matter **53**, 16067 (1996).
36. J. G. Chen, Surf. Sci. Rep. **30**, 1 (1997).

*Translated by A. Kazantsev*